ORIGINAL ARTICLE

Melatonin alleviates alcoholic liver disease *via* EGFR−BRG1−TERT axis regulation

Zhaodi Che[a], Yali Song[a], Chengfang Xu[b], Wei Li[c], Zhiyong Dong[a], Cunchuan Wang[a], Yixing Ren[d], Kwok-Fai So[e], George L. Tipoe[f], Fei Wang[g,*], Jia Xiao[a,f,*]

[a]*Clinical Medicine Research Institute and Department of Metabolic and Bariatric Surgery, the First Affiliated Hospital of Jinan University, Guangzhou 510632, China*
[b]*Department of Obstetrics, the Third Affiliated Hospital, Sun Yat-sen University, Guangzhou 510630, China*
[c]*Faculty of Pharmaceutical Sciences, Toho University, Chiba 2748510, Japan*
[d]*Department of General Surgery, and Institute of Hepato-Biliary-Pancreas and Intestinal Disease, Affiliated Hospital of North Sichuan Medical College, Nanchong 637000, China*
[e]*GMH Institute of CNS Regeneration, Guangdong Medical Key Laboratory of Brain Function and Diseases, Jinan University, Guangzhou 510632, China*
[f]*School of Biomedical Sciences, LKS Faculty of Medicine, the University of Hong Kong, Hong Kong, China*
[g]*Division of Gastroenterology, Seventh Affiliated Hospital of Sun Yat-sen University, Shenzhen 518107, China*

Abstract Chronic alcohol consumption causes liver steatosis, cell death, and inflammation. Melatonin (MLT) is reported to alleviate alcoholic liver disease (ALD)-induced injury. However, its direct regulating targets in hepatocytes are not fully understood. In the current study, a cell-based screening model and a chronic ethanol-fed mice ALD model were used to test the protective mechanisms of MLT. MLT ameliorated ethanol-induced hepatocyte injury in both cell and animal models (optimal doses of 10 μmol/L and 5 mg/kg, respectively), including lowered liver steatosis, cell death, and inflammation. RNA-seq analysis and loss-of-function studies in AML-12 cells revealed that telomerase reverse transcriptase (TERT) was a key downstream effector of MLT. Biophysical assay found that epidermal growth factor receptor (EGFR) on the hepatocyte surface was a direct binding and regulating target of MLT. Liver specific knock-down of *Tert* or *Egfr* in the ALD mice model impaired MLT-mediated liver protection, partly through the regulation of nuclear brahma-related gene-1 (*BRG1*). Long-term administration (90 days) of MLT in healthy mice did not cause evident adverse effect. In conclusion, MLT is an efficacious and safe agent for ALD

---

*Corresponding authors.
E-mail addresses: edwinsiu@connect.hku.hk (Jia Xiao), wangf323@mail.sysu.edu.cn (Fei Wang).

alleviation. Its direct regulating target in hepatocytes is EGFR and downstream BRG1−TERT axis. MLT might be used as a complimentary agent for alcoholics.

1. Introduction

Excessive ethanol consumption (alcohol abuse) is a leading cause of alcoholism, malnutrition, chronic pancreatitis, alcoholic liver disease (ALD) and cancer. ALD is an umbrella term for a range of liver conditions from simple steatosis, alcoholic steatohepatitis, to alcoholic cirrhosis[1]. The United States and European countries have a notable prevalence of ALD (∼6%), and that in China (∼4.5%) and Japan (1.56%−2.34%) is also increasing due to remarkably increased ethanol consumption[2]. To date, abstinence and nutrition supports are the major therapies for ALD, although their clinical application has met several difficulties. Corticosteroids, the current first-line treatment for severe alcoholic steatohepatitis have remained controversial clinical efficacy because of the marginal short-term survival benefit[3]. The pathological progression of ALD is driven by multiple mechanisms, including lipid accumulation, inflammation, oxidative stress, and necro-apoptosis. However, other critical contributing signaling pathways for steatosis to inflammation transition, gut−liver crosstalk, and fibrotic resolving, which are important for the development of targeted therapy, are unfortunately not fully understood[4].

Telomerase is a ribonucleoprotein consists of telomerase RNA and telomerase reverse transcriptase (TERT). Most adult cells, including those in the liver, display low basal telomerase activity and low expression level of TERT due to telomeres shorten as a result of the incomplete replication of linear chromosomes. Emerging evidence suggests telomerase reactivation is involved in liver cirrhosis and hepatocellular carcinoma[5,6]. In metabolic liver diseases, telomerase enzyme deficiency promotes metabolic dysfunction in murine hepatocytes, and antioxidant treatment improves fatty liver *via* activating telomerase[7,8]. In addition, TERT is reported to act in a feedback loop with nuclear factor kappa B (NF-κB) pathway to regulate macrophage polarization in ALD[9]. However, roles of hepatocyte TERT in ALD progression remains largely unknown.

Melatonin (*N*-acetyl-5-methoxytryptamine, MLT) is a hormone mainly synthesized by the pineal gland. MLT plays central roles in the body's sleep−wake cycle. The production of MLT increases with evening darkness to promote healthy sleep and help to orient precise circadian rhythm[10]. Recent studies have revealed that disruption of melatonin secretion was associated with metabolic disorders, such as type 2 diabetes[11] and non-alcoholic fatty liver disease (NAFLD)[12]. Supplementation with 6 mg melatonin (1 h before bedtime) of melatonin for 12 weeks significantly improved NAFLD symptoms such as NAFLD score, liver enzymes and anthropometric measurements in a randomized double blind clinical trial[13]. For ALD, there was a study claimed that treatment with melatonin significantly attenuated ethanol-induced hepatocyte steatosis and the immigration of inflammatory cells in mice[14]. Whereas the application of hormone in the treatment of ALD has been at the forefront of investigation[15−17], the possible role for cell surface receptor in the protection has received little attention. Although ethanol is a small molecule that diffuses easily across cell membranes, it does regulate the biological functions of many cell surface receptors. For example, direct binding of gamma-aminobutyric acid A receptor has been reported in ethanol-induced behavioral alterations[18]. Ethanol also regulates toll-like receptor (TLR)-mediated signaling in macrophage, possibly by altering lipid rafts in the liver[19]. Recently we identified the divergent roles of Kupffer cell TLR2 and TLR3 in an ALD mice model, as well as the direct binding and regulation of them by epigallocatechin gallate derived from green tea[20]. In the current study, we aimed to test the hepatoprotective roles of MLT in both *in vitro* and *in vivo* ALD models. The direct binding target—epidermal growth factor receptor (EGFR) of MLT on the hepatocyte surface was confirmed by using biophysical assays. Downstream brahma-related gene-1 (*BRG1*)-TERT pathway regulated by ethanol and MLT was revealed using RNA-seq and specific knock-down methods.

2. Materials and methods

2.1. Chemicals and reagents

MLT powder (≥98% purity; #M5250) were purchased from Sigma−Aldrich (St. Louis, MO, USA). Pure ethanol was purchased from Guangzhou Chemical Reagent Factory (Guangzhou, China). All cell culture consumables and reagents were supplied by either Corning Incorporated (Corning, NY, USA) or Gibco (Carlsbad, CA, USA). Primary antibodies against phosphorylated Akt at Thr 308 or Ser473 (#ab38449 and #ab81283), total Akt (#ab8805), beta-actin (β-actin, #ab8226), BRG1 (#ab110641), cleaved caspase-3 (#ab2302), Cyclin D1 (#ab16663), cytochrome *c* (Cyto C; #ab133504), phosphorylated EGFR at Tyr1068 (#ab40815), total EGFR (#ab52894), interleukin-6 (IL-6; #ab259341), phosphorylated NF-κB p65 subunit at Ser536 (#ab76302), total p65 (#ab16502), proliferating cell nuclear antigen (PCNA; #ab92552), sterol regulatory element-binding protein 1c (SREBP-1c; # ab28481), tumor necrosis factor-α (TNF-α; #ab183218), and TERT (#ab191523) were purchased from Abcam (Cambridge, UK). All antibodies are validated by their manufacturers (see corresponding product web pages) and in our pilot studies.

2.2. Construction of AAV8-shRNAs

Adeno-associated virus 8 (AAV8) was produced by transfection of AAV-293 cells with three plasmids namely an AAV vector expressing the shRNA to mouse *Tert* or *Egfr*, AV helper plasmid (pAAV Helper) and AAV Rep/Cap expression plasmid. After transfection for 72 h, cells were collected and lysed using a freeze-thaw procedure. Viral particles were purified by an iodixanol step-gradient ultracentrifugation method. AAV was concentrated using a 100 kDa molecular-mass-cut off ultrafiltration device. The

genomic titer was $2.5 \times 10^{12}-5 \times 10^{12}$ infectious units per mL as determined by quantitative PCR. To construct shRNAs, oligonucleotides that contained sense and antisense sequences were connected with a hairpin loop followed by a poly(T) termination signal. The sequence of the control shRNA was TTCTCCGA ACGTGTCACGT. These shRNAs were ligated into an AAV8 vector expressing H1 promoter and EGFP.

2.3. Cell culture and transfection

The mouse normal hepatocyte line AML-12 was purchased from the Cell Bank of Type Culture Collection of Chinese Academy of Sciences (Shanghai, China). Cells were cultured in Dulbecco's modified Eagle's medium with 10% (v/v) fetal bovine serum at 37 °C with 5% CO_2 using a cell incubator. Cells were treated after they reached a confluence of 60%−70%. To induce in vitro ALD-like injury of AML-12 cells, we co-treated cells with 50−1000 mmol/L ethanol and 0.1−1 mmol/L palmitate acid (PA; Sigma−Aldrich; #P0500) for 24 h to find out the best concentration combination, as we previously reported[21,22]. After that, different doses of MLT were added along with concurrent PA and ethanol for a 24 h incubation to rule out the optimal dose of MLT. Knockdown of Tert, Rbp1, Rnaseh2c, Espn, Iba57, Brg1 were achieved by transfection of Rosetta Predictions siRNA (Sigma−Aldrich; #NM_009354, #NM_011254, #NM_026616, #NM_019585, #NM_001270791, #NM_001174079, respectively) with Lipofectamine 3000 reagent (Thermo-Fisher, Waltham, MA, USA; #L3000001).

2.4. RNA sequencing and functional enrichment analysis

Total RNA was isolated from cells/tissues using the Trizol (Invitrogen, Carlsbad, CA, USA) according to the manufacturer's protocol. RNA purity was assessed using the ND-1000 Nanodrop (ThermoFisher, Waltham, MA, USA). Each RNA sample had an A_{260}:A_{280} ratio above 1.8 and A_{260}:A_{230} ratio above 2.0. RNA integrity was evaluated using the Agilent 2200 TapeStation (Agilent Technologies, Santa Clara, CA, USA) and each sample had the RIN above 7.0. Briefly, rRNAs were removed from Total RNA using EpicentreRibo-Zero rRNA Removal Kit (Illumina, San Diego, CA, USA) and fragmented to approximately 200bp. Subsequently, the purified RNAs were subjected to first strand and second strand cDNA synthesis following by adaptor ligation and enrichment with a low-cycle according to instructions of NEB-Next Ultra RNA Library Prep Kit for Illumina (New England Biolabs, Ipswich, MA, USA). The purified library products were evaluated using the Agilent 2200 TapeStation and Qubit2.0 (ThermoFisher) and then diluted to 10 pmol/L for cluster generation in situ on the pair-end flow cell followed by sequencing $(2 \times 150$ bp) HiSeq3000.

The clean reads were obtained after removal of reads containing adapter, ploy-N and at low quality from raw data. HISAT2 was used to align the clean reads to the mouse reference genome mm10 with default parameters. HTSeq was subsequently employed to convert aligned short reads into read counts for each gene model. Differential expression was assessed by DESeq using read counts as input. The Benjamini−Hochberg multiple test correction method was enabled. Differentially expressed genes were chosen according to the criteria of fold change > 2 and adjusted P value < 0.05. All the differentially expressed genes were used for heat map analysis and Kyoto Encyclopedia of Genes and Genomes (KEGG) ontology enrichment analyses. For KEGG enrichment analysis, a P value < 0.05 was used as the threshold to determine significant enrichment of the gene sets.

2.5. Cell lipid accumulation, viability, apoptosis assays

To visualize the intracellular lipid droplets, AML-12 cells were washed by sterile phosphate buffer saline (PBS), and then stained with Nile Red solution (0.1 mg/mL; #N8440, Solarbio, Beijing, China) at 37 °C for 20 min. After that, cells were fixed with 4% formaldehyde for 10 min, and then counterstained with DAPI (5 μg/mL; Sigma−Aldrich) for 10 min. The 3-(4,5-dimethyl-thiazol-2-yl)-2,5-diphenyl-tetrazolium bromide (MTT) cell viability assay was conducted as described in previous report[22]. After drug treatment, Hoechst 33342 (5 μg/mL; Sigma−Aldrich) and propidium iodide (5 μg/mL; Sigma−Aldrich) were added to each well to stain live cells. Quantifications of apoptotic ratio were conducted as previously described[23].

2.6. Caspase-3/7 activity assay

Activities of caspases-3/7 from cell lysates after treatment were measured using Cell Meter Caspase 3/7 Activity Apoptosis Assay Kit (AAT Bio., Sunnyvale, CA, USA; #22795) according to the user manual. Final results were read at 520 nm in a micro-plate reader (Bio-Rad) and expressed as fold change in caspase-3/7 activity relative to the control.

2.7. Quantitative real-time PCR

Total RNA was extracted from fresh liver tissue samples or cell lysates by using the CellAmp Direct RNA Prep Kit (Takara Bio Inc., Shiga, Japan; #3732). The first strand cDNA was synthesized from total RNA using a PrimeScript RT Reagent Kit (Takara; #RR037) following the manufacturer's instructions. qPCR reaction was performed with the SYBR Premix Taq Quantitative PCR Kit (Takara Bio Inc., Shiga, Japan) according to the manufacturer's instructions, on a MyiQ2 real-time quantitative PCR machine (Bio-Rad, Berkeley, CA, USA). Primer information is as listed in Supporting Information Table S1. Glyceraldehyde-3-phosphate dehydrogenase (Gapdh) was amplified as an internal control. The relative quantification of mRNA expression levels was done according to the $2^{-\Delta\Delta Ct}$ method. All real-time PCR procedures, including the design of primers, validation of PCR environment and quantification methods, were performed according the MIQE guideline[24].

2.8. Animals and experimental design

Male C57BL/6 wild-type mice (7-weeks-old; ~ 20 g) were purchased from Guangdong Medical Animal Centre (Guangzhou, China). Mice were acclimatized to their environment for 1 week before the experiments. Alcoholic liver injury was induced by using the National Institute on Alcohol Abuse and Alcoholism (NIAAA) model with minor modifications[25]. Briefly, mice (10/group) were initially fed ad libitum with the control Lieber-DeCarli diet for 5 days to allow acclimation to liquid diet. Then, the ALD group mice (indicated as 'EtOH' group in figures) were fed with the Lieber-DeCarli diet containing 5% (v/v) ethanol for 10 days (first stage), while the control mice (indicated as 'Pair' group in figures) were pair-fed with the isocaloric control diet (same caloric content). Changes in body weight and food intake of each mouse were recorded every day. On Day 11, ethanol-fed and

pair-fed mice were fed by gavage method in the early morning with a single dose of ethanol (the binge consumption; 5 g/kg body weight) or isocaloric maltose dextrin, respectively, and euthanized 9 h later. For viral infections, mice were injected *via* the tail vein with 1×10^{12} genome copies of AAV8 control or AAV-shRNA (five per group). After 14 days, mice were fasted for 4 h at the end of the dark cycle and then sacrificed to ensure the hepatic down-regulation of *Tert, or Egfr*. These mice were also subjected to NIAAA model and/or MLT administration as described above. Target gene expression has been verified using PCR in the liver and other tissues, including brain, heart, white adipose tissue (WAT), and skeletal muscle, as we previously reported[26]. All experimental procedures were approved by the Ethical Committee of Jinan University, China.

2.9. Serum/hepatic biochemistry and cytokine measurements

Serum levels of alanine aminotransferase (ALT), aspartate aminotransferase (AST), triglyceride (TG) and total cholesterol (TC) were measured using Hitachi LABOSPECT 008 (Hitachi High-Tech Co., Tokyo, Japan). Serum and hepatic cytokine levels were determined by using corresponding ELISA kits from Peprotech (Rocky Hill, NJ, USA; TNF-α: #900-M54; IL-6: #900-M50). Hepatic TG contents were measured by a colorimetric TG assay kit from Sigma−Aldrich (#MAK266).

2.10. Tissue histology

Tissues were fixed in 10% phosphate-buffered formalin and embedded in paraffin blocks. A thickness of 5 μm of tissue section was cut and stained with hematoxylin and eosin (H&E) and Oil Red O (Sigma−Aldrich) for histological analysis using a LEICA Qwin Image Analyzer (Leica Microsystems Ltd., Milton Keynes, UK). The NAFLD activity score (NAS) of each group was calculated as previously described[27].

2.11. Respiratory exchange ratio and energy expenditure

Respiratory exchange ratio (RER) and energy expenditure were measured by using a Comprehensive Laboratory Animal Monitoring System (Columbus Instruments, Columbus, OH, USA). Five mice per group were housed individually and assessed by indirect calorimetry over 48 h (last 2 days of the NIAAA model) and maintained at 24 °C under at 12-h:12-h light−dark cycle. An RER of 0.7 indicates that fat is the predominant fuel source, while an RER closer to 1.0 indicates that carbohydrate is the primary fuel[28].

2.12. Telomerase activity assay

Measurement of telomerase activity was conducted by using protocols as previously described[29]. The telomerase products (6 bp ladder) and the 36 bp internal control bands were quantified by ImageJ software (National Institute of Health, Bethesda, MD, USA). Relative telomerase activity was calculated from the intensity ratio between the TRAP ladder to internal control band.

2.13. Protein structure modeling and molecular docking

Since the crystal structure of mouse EGFR was not available, we used human EGFR data from the Protein Data Bank (PDB) database (PDB code: 3gop; sequence similarity 98.31%) for

modeling[30]. The modeling of protein homology of mouse EGFR structure has passed the quality check of SAVES website toolkits (version 6.0; https://saves.mbi.ucla.edu). The protein−ligand docking studies between EGFR and melatonin were based on these obtained compound structures and carried out with Auto-dock Vina (version 1.2.0). First, polar hydrogen atoms and Gasteiger charges were added to ligand, and non-polar hydrogen atoms were merged using AutoDock Tools software (ADT, version 1.5.6) before docking analysis. The GetBox plugin was used to design box (X: −7.0, Y: −21.0, Z: −40.0) with EGFR as the center, and then part of EGFR was set as the target for a global search using AutoDock Vina to identify the best binding site. Then we chose the docking conformation with the lowest binding energy, by PyMol, to visualize the protein-ligand docking conformation[31].

2.14. Surface plasmon resonance (SPR) assay

To verify the molecular docking results, we bought recombinant murine EGFR protein (extracellular domain, position 25−647 of the total EGFR protein; HEK293 cell produced; Abcam, #ab167752) and expressed/purified the cytoplasmic domain (position 671−1210 of the total EGFR protein) by using the HEK293 system. Analysis of direct interactions between MLT and extracellular/cytoplasmic domains of EGFR was performed at 25 °C on a BIAcore T200 SPR instrument (GE Healthcare, Boston, MA, USA). SPR running buffer contained 50 mmol/L HEPES (pH 7.5), 150 mmol/L NaCl, 3 mmol/L EDTA and 0.005% (*v/v*) Tween-20 and was prepared immediately before measurement. BIAcore sensor chip CM5 (#29104988) was activated for 5−10 min in a 1:1 mixture of 0.1 mol/L *N*-hydroxysuccinimide and 0.1 mol/L *N*-ethyl-*N'*-(3-diethylaminopropyl)-carbodiimideat a flow rate of 10 μL/min. Recombinant mouse EGFR protein was immobilized *via* amine coupling on a flow cell of the chip. The remaining binding sites on the chips were blocked by 1 mol/L ethanolamine (pH 8.5) at a flow rate of 10 μL/min for 5 min. Control sensorgrams, obtained on an empty flow cell where the coupling reaction had been conducted in the presence of coupling buffer alone, were always subtracted from binding responses. MLT was diluted in the running buffer and then injected at different concentrations (31.25−1000 nmol/L for the cytoplasmic domain and 125−4000 μmol/L for the extracellular domain) and passed over adjacent target and control flow cells at a flow rate of 20 μL/min for 180 s. After a 5-min dissociation, the bound analytes were removed by a 20-s wash with 20 mmol/L NaOH[32].

2.15. Protein extraction and Western blot

After treatments, cells or liver tissues were washed with sterile PBS for three times and then subjected to total protein extraction by using a RIPA kit from Sigma−Aldrich. For secreted protein, culture medium was collected and centrifuged for RIPA extraction. Then protein samples were quantified with BCA reagent from Bio-Rad. Western blot analyses of all proteins were performed as described using β-actin as the internal control.

2.16. Statistical analysis

Data from each group are expressed as mean $\pm$ standard deviation (SD). For normally distributed data, statistical comparisons were carried out using unpaired two-tailed Student's *t*-test for two group comparisons; for three or more group comparisons, two-way

ANOVA was used with a Student-Newman-Keuls *post hoc* test (Prism 5.0, Graphpad software, Inc., San Diego, CA, USA). A value of $P < 0.05$ was considered to be statistically significant.

3. Results

3.1. MLT alleviates ethanol-induced hepatocyte injury in vitro

Since MLT (Fig. 1A) was reported to alleviate oxidative stress, inflammatory response, and apoptosis in a mice ALD model without answering the concrete pathways, we further explored its underlying mechanisms and the direct regulating membrane receptor in the current study. In an ethanol/PA concomitantly induced AML-12 hepatocyte injury *in vitro* model, *via* a series of concentration combination pilot experiments, it was determined that 250 mmol/L ethanol and 0.25 mmol/L PA as the best concurrent treatment doses to induce evident alcoholic cell death and lipid accumulation in AML-12 cells (Supporting Information Fig. S1). Co-treatment with MLT (10–50 μmol/L) exhibited improvement on cell viability, lipid accumulation, and apoptosis in a dose-dependent manner (Fig. 1B–D). Ethanol/PA treatment significantly elevated the expression of lipogenic genes (*Srebp-1c* and *Acc*) while inhibited the expression of lipolytic gene (*AdipoQ*). MLT co-treatment, as expected, evidently re-balanced the lipid metabolism of AML-12 cells (Fig. 1E). Moreover, MLT dose-dependently reduced the production of pro-inflammatory cytokines (TNF-α and IL-6) induced by ethanol/PA treatment at both transcriptional and translational levels (Fig. 1F). Since 10 μmol/L was the minimal effective dose of MLT for AML-12 protection, we used this dosage in the immunoblot assay and all following *in vitro* studies.

3.2. Tert is involved in ethanol-induced hepatocyte injury and MLT-mediated protection in vitro

To further investigate major involving pathways and targets in MLT-mediated protection against ethanol/PA treatment, we collected AML-12 lysates for RNA-seq analysis. When the threshold criteria were set, it was shown that ethanol/PA up-regulated 5288 genes (top 5: *Il6*, *Gbp5*, *Csf3*, *Lif*, and *Il1b*) while down-regulated 11,845 genes (top 5: *Osbpl6*, *Cbfa2t3*, *Vipr1*, *Tert*, and *Ranbp3l*). Further addition with 10 μmol/L MLT up-regulated 155 genes (top 5: *Lama5*, *Rbp1*, *Tert*, *Stum*, and *Rnaseh2c*) while down-regulated 226 genes (top 5: *Espn*, *Zfp663*, *Cldn7*, *Col6a3*, and *Iba57*). Immune and metabolic pathways were top pathways regulated by ethanol/PA and MLT (Fig. 2A; Supporting Information Table S2). Since roles of pro-inflammatory cytokines (*e.g.*, *Il6* and *Il1b*) have been substantially studied in ALD[33], we selected 8 genes for quantitative PCR validation. Results showed that mRNA expressions of *Tert*, *Rbp1*, *Rnaseh2c*, *Espn*, and *Iba57* were significantly influenced by ethanol/PA treatment but reversed by MLT co-treatment (Fig. 2B). Thus, by using specific siRNAs, we observed the effects of knock-down of *Tert*, *Rbp1*, *Rnaseh2c*, *Espn*, and *Iba57* on AML-12 cell lipid accumulation and apoptosis. As shown in Fig. 2C, transfection with siRNA successfully knocked-down the mRNA levels of those genes without influencing cell viability. Unlike *Rnaseh2c*, *Espn*, and *Iba57*, knock-down of *Tert* and *Rbp1* significantly rescued ethanol/PA treatment-induced cellular lipid accumulation and apoptosis (Fig. 2D). Because *Tert* was the only gene that was evidently inhibited by ethanol/PA treatment and elevated by MLT, we then

focused its mechanistic involvement in MLT-mediated hepatocyte protection. Inhibition of endogenous *Tert* expression abolished MLT-induced lipid metabolism re-balance, which was shown by Nile Red staining and mRNA expressional changes of lipogenic/lipolytic genes (*Srebp-1c*, *Acc*, and *AdipoQ*) (Fig. 3A–C). This was further confirmed by protein level changes of TNF-α and IL-6 within and released from AML-12 hepatocytes (Fig. 3D). Since TERT is reported to promote liver regeneration after injury[34,35], we then measured expressional changes of liver regeneration markers, *Osm*, *Osmr*, PCNA, and Cyclin D1, which showed that MLT drastically recovered AML-12 regeneration impaired by ethanol/PA treatment. Knockdown of *Tert* abolished such effects (Fig. 3E). Collectively, *Tert* is involved in ethanol-induced hepatocyte injury and MLT-mediated protection.

3.3. EGFR–Akt–BRG1 directly transduces MLT-mediated protection signal in hepatocytes

To further elucidate the upstream signaling events of TERT, we firstly explored the involvement of a direct binding protein of TERT–BRG1 (SMARCA4) in AML-12 cells[36]. Its protein level was elevated after ethanol/PA intoxication but prohibited by the co-treatment with MLT (Fig. 4A). In addition, when endogenous *Brg1* was knocked-down by siRNA in AML-12 cells, both the mRNA level of *Tert* and telomerase activity were significantly promoted, indicating an inverse regulation between BRG1 and TERT (Fig. 4B and C). Since EGFR–Akt was reported to directly regulate BRG1 activity[37], we then investigated the activity changes of this pathway in AML-12 cells with or without *Tert* knockdown. Treatment with ethanol/PA inhibited the phosphorylation of both EGFR and Akt, which were partially recovered by the co-treatment with MLT but abolished by the knock-down of *Tert*, implying that *Tert* was essential for upstream EGFR–Akt autophosphorylation (Fig. 4D)[38]. Consistently, inhibition of Akt by LY294002 significantly reduced BRG1 activation and recovered Cyclin D1 expression after ethanol/PA treatment, and could not exhibit further contribution to MLT-mediated beneficial effects on the BRG1–Cyclin D1 regulation (Fig. 4E). This result suggested that Akt was indispensable for MLT-mediated hepatocytes protection. To test the possible direct binding between MLT and EGFR, we firstly investigated the possible interactions between the EGFR kinase domain and MLT by molecular docking analysis. The docking results revealed that MLT formed carbon hydrogen bond with the residues of Leu863 and Ala866, conventional hydrogen bond with Phe858 and Glu870, π–alkyl bond with Phe725, and π–cation bond with Lys869, all of which were the catalytic binding sites of the cytoplasmic domain of EGFR protein (Fig. 4F). To further characterize the specific binding sites, we tested the direct binding between MLT and the recombinant extracellular domain or the cytoplasmic domain of mouse EGFR protein expressed by the eukaryotic HEK293 system using SPR. It was demonstrated that MLT directly bound to the cytoplasmic ($K_d = 4.41 \times 10^{-4}$) instead of the extracellular domain ($K_d = 1.78 \times 10^{-2}$) of EGFR (Fig. 4G). Those results were consistent with previous studies showing that small-molecule inhibitors (*e.g.*, gefitinib) could primarily target the catalytic binding sites within the cytoplasmic domain of EGFR to regulate downstream pathways[39,40]. Importantly, since the key molecules [the adenylyl cyclase (AC)-cyclic adenosine monophosphate (cAMP) pathway and the protein kinase C (PKC) cascade] of the melatonin MT$_1$ and MT$_2$ receptor downstream pathways were not significantly altered, as demonstrated by the RNA-seq results (Table S2),
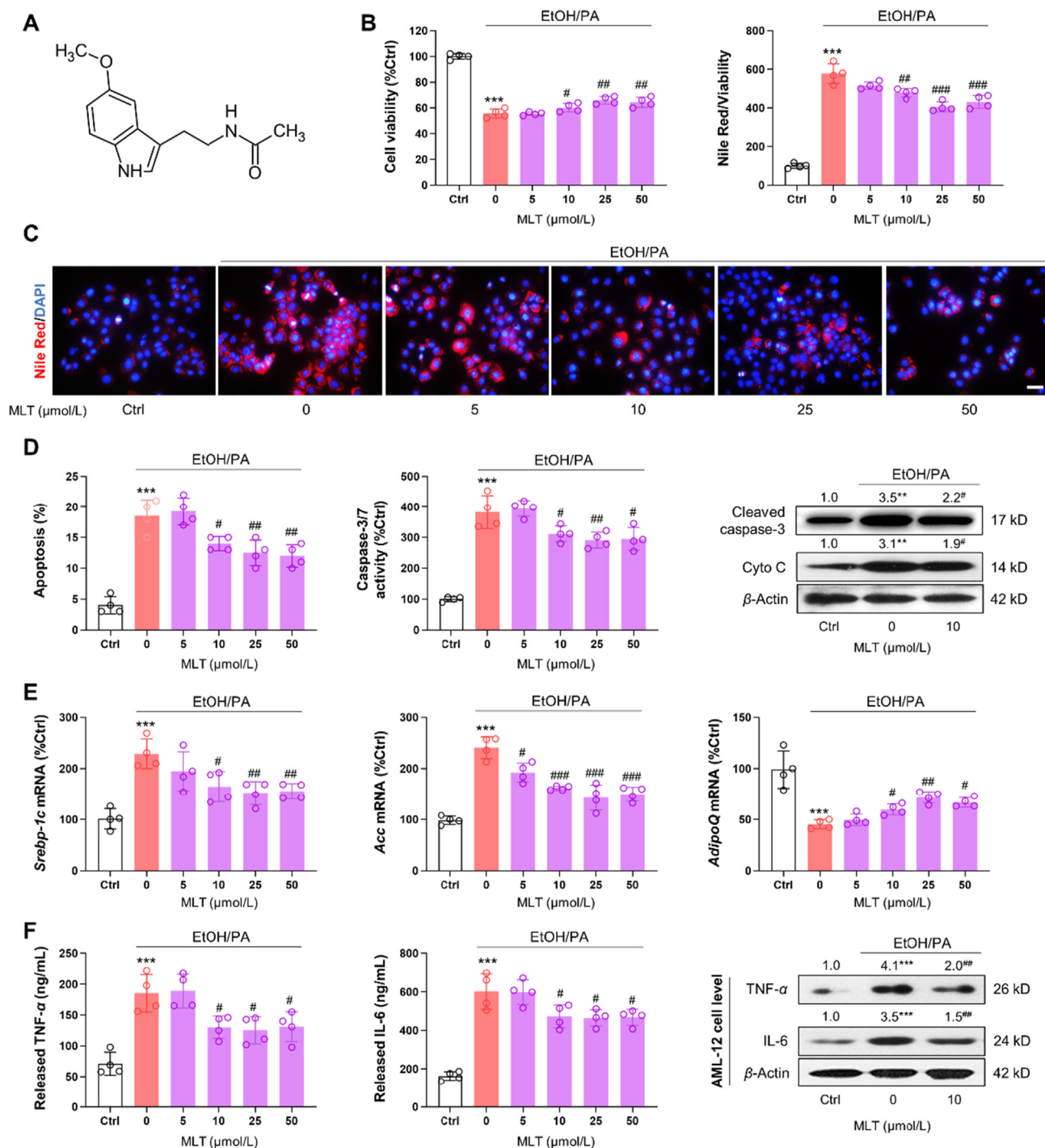
Figure 1 Effects of melatonin (MLT) on cell injury in an ethanol/palmitate acid (PA) concomitantly induced AML-12 hepatocyte model. (A) Chemical structure of MLT (*N*-acetyl-5-methoxytryptamine). (B) Changes of AML-12 cell viability and cellular Nile Red staining signal after ethanol/PA treatment in the absence or presence of different doses (0, 5, 10, 25, 50 μmol/L) of MLT co-treatment (*n* = 4). (C) Representative Nile Red staining images of AML-12 cells treated with ethanol/PA in the absence or presence of different doses of MLT co-treatment. (D) Changes of apoptotic percentage, cellular caspase-3/7 activity, cleaved caspase-3 protein level, and cytochrome *c* (Cyto C) protein level of AML-12 cells treated with ethanol/PA in the absence or presence of different doses of MLT co-treatment (*n* = 4 for apoptotic percentage and cellular caspase-3/7 activity; *n* = 3 for Western blotting). (E) Results of cellular mRNA level changes of *Srebp-1c*, *Acc*, and adiponectin (*AdipoQ*) of AML-12 cells treated with ethanol/PA in the absence or presence of different doses of MLT co-treatment (*n* = 4). (F) ELISA results of released TNF-α and IL-6 protein from AML-12 cells and cellular TNF-α and IL-6 protein of AML-12 cells treated with ethanol/PA in the absence or presence of different doses of MLT co-treatment (*n* = 4 for ELISA results; *n* = 3 for Western blotting). Data are expressed as mean SDs. ***$P < 0.001$ *vs.* the control group; #$P < 0.05$, ##$P < 0.01$, ###$P < 0.001$ *vs.* the ethanol/PA group. Scale bar: 50 μm.
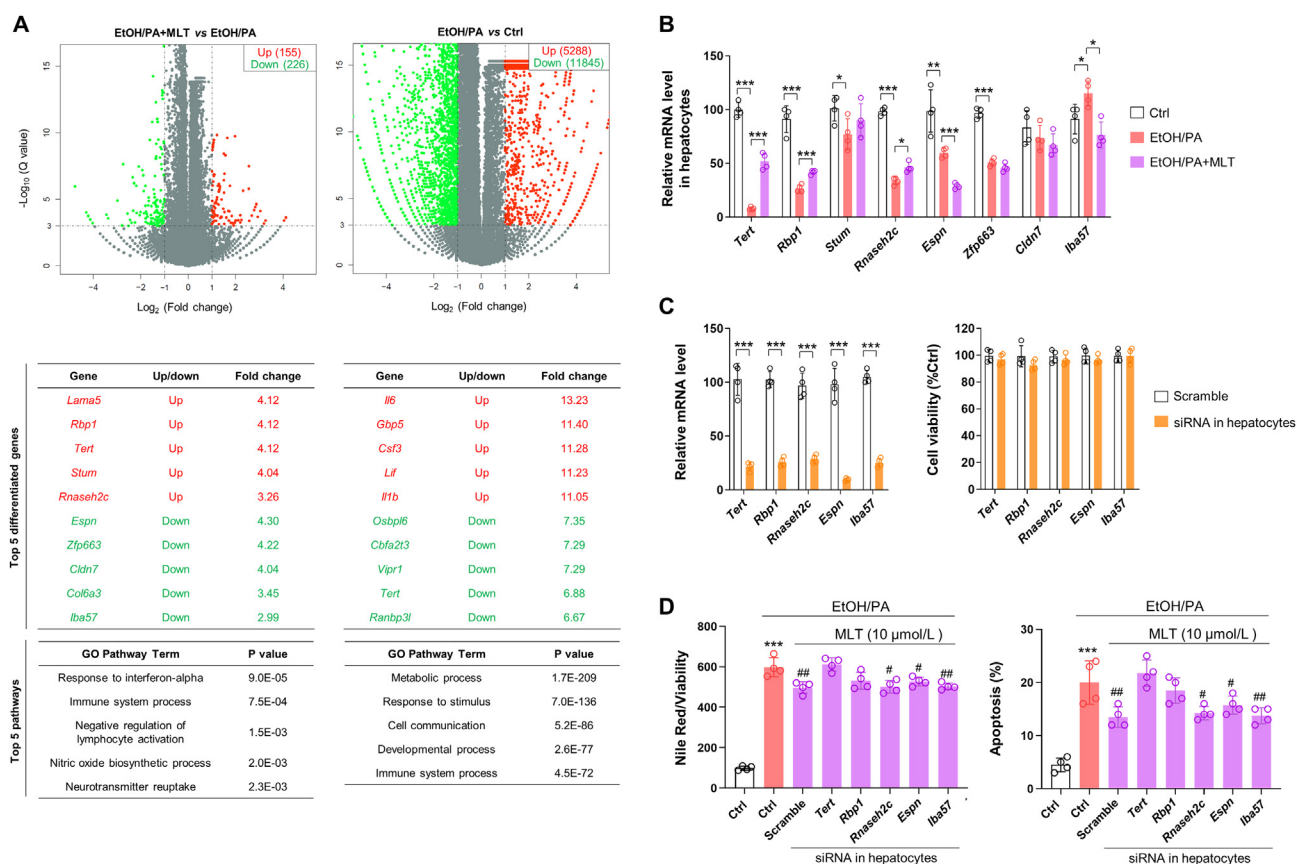
Figure 2 TERT is involved in ethanol/palmitate acid (PA) concomitantly induced AML-12 hepatocyte damage and MLT protection. (A) Volcano analysis results of differentially expressed genes in EtOH/PA + MLT *vs.* EtOH/PA groups and EtOH/PA *vs.* control (Ctrl) groups after RNA-seq of AML-12 cells. Top 5 differentiated genes (both up-regulated and down-regulated) and top 5 regulated pathways were also shown. (B) Quantitative PCR validation of RNA-seq exhibited top differentiated genes in AML-12 cells treated with ethanol/PA in the absence or presence of 10 μmol/L MLT (*n* = 4). (C) Quantitative PCR results of knock-down efficiency by siRNAs of genes in AML-12 cells. Changes of AML-12 cell viability after siRNA transfection (24 h) were also tested (*n* = 4). (D) Changes of cellular Nile Red staining signal/cell viability ratio and apoptotic ratio of AML-12 cells treated with ethanol/PA in the absence or presence of 10 μmol/L MLT, and knock-down of specified genes (*n* = 4). Data are expressed as mean ± SD. *$P < 0.05$, **$P < 0.01$, ***$P < 0.001$ between indicated groups. For panel D, ***$P < 0.001$ *vs.* the control group; #$P < 0.05$, ##$P < 0.01$ *vs.* the ethanol/PA group.

we did not test the involving roles of hepatocyte MT_1 and MT_2 in this animal model.

3.4. MLT improves liver injury in a mouse ALD model

In a well-recognized chronic-binge ALD mouse model (the NIAAA model), we firstly tested the optimal dose of daily gavaged MLT by using 1, 5, and 10 mg/kg doses in our pilot study. Histological NAS scores and serum ALT/AST results showed that 5 and 10 mg/kg had similar significant improvements in liver injury without influencing healthy mice. Thus, we used 5 mg/kg MLT in the following animal studies (Supporting Information Fig. S2). When compared with the pair group fed with normal diet, ethanol consumption caused significantly slower the increase of body weight and reduced RER/energy expenditure, although the food intake was similar. Administration with MLT partially recovered the gain of body weight, RER, and energy expenditure without influencing healthy mice (Fig. 5A and Supporting Information Fig. S3). The liver of the ALD group mice exhibited typical histological abnormalities, including fat droplet accumulation and macrophage infiltration, leading to an increased NAS

score. MLT co-treatment effectively alleviated such changes (Fig. 5B and C). Of note, serum chemical tests of liver function (ALT and AST), lipid metabolism (TC and TG), and systemic inflammation (TNF-α and IL-6) exhibited similar results (Fig. 5D and E). In line with the AML-12 cell finding, mice with ALD showed inhibited hepatic *Tert* expression and telomerase activity, which were also partially restored by MLT consumption (Fig. 5F). Protein expressional changes of hepatic apoptosis marker (cleaved caspase-3 and cytochrome *c*), EGFR–Akt–BRG1 axis, liver regeneration (Cyclin D1), inflammation (phosphorylated NF-κB p65 subunit), and lipid metabolism (SREBP-1c) suggested that MLT evidently improved hepatic injury and promoted liver regeneration *via*, at least a partial, regulation of the EGFR–Akt–BRG1 pathway (Fig. 5G).

3.5. MLT alleviates alcoholic liver disease via the EGFR–BRG1–TERT axis

To further characterize the involving role of TERT in the mice ALD model, we specifically knocked down its expression in hepatocytes by using AAV8-packaged shRNA (Fig. 6A). Deficiency
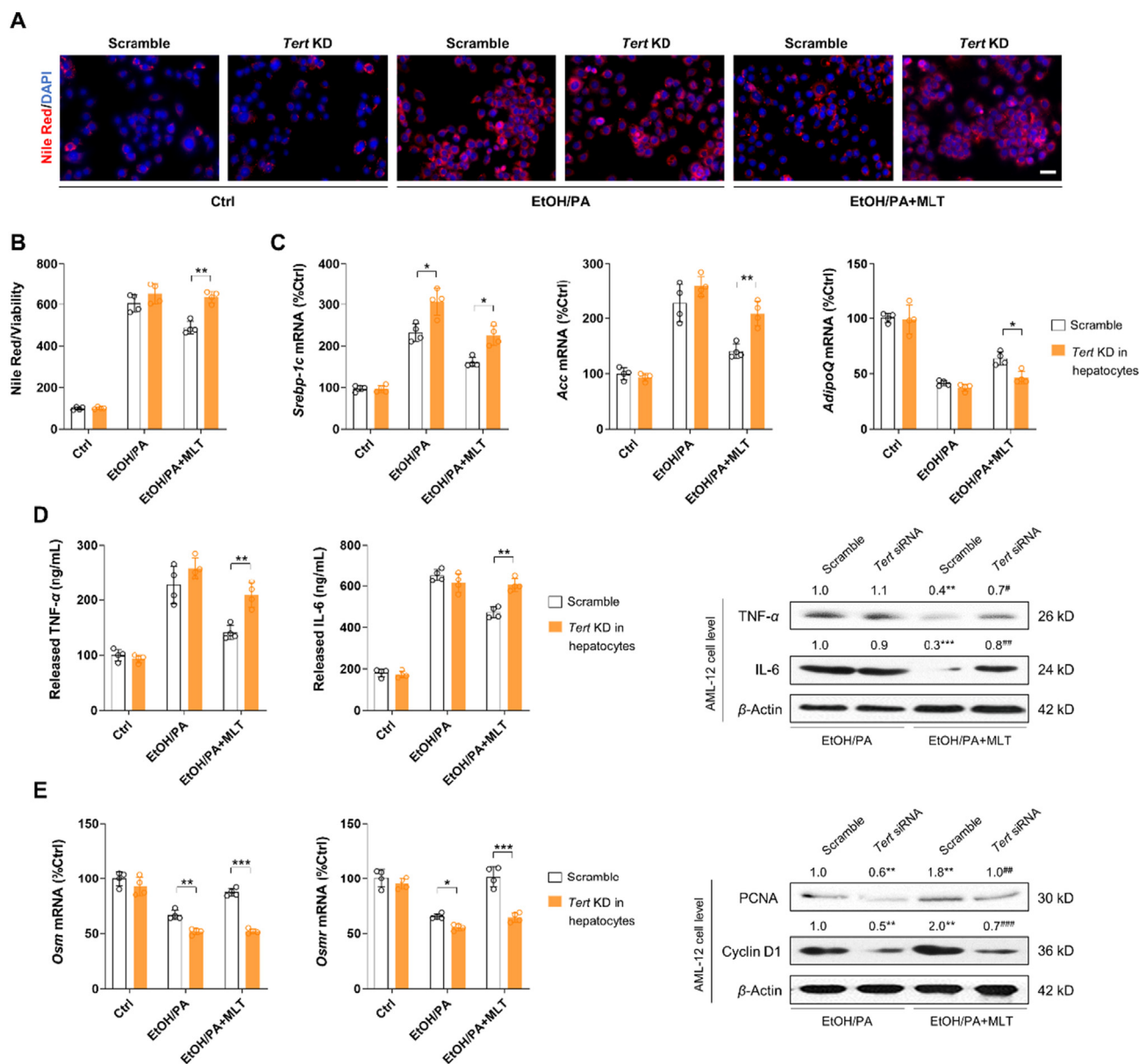
Figure 3 Knock-down of *Tert* impairs MLT-mediated protection against ethanol/palmitate acid (PA)-induced AML-12 damage. (A, B) Nile Red staining signal/cell viability ratio with representative cell staining images and (C) mRNA level of key lipid metabolism genes (*Srebp-1c*, *Acc*, and *AdipoQ*) of AML-12 cells treated with ethanol/PA in the absence or presence of 10 μmol/L MLT, and knock-down (KD) of *Tert* (*n* = 4). (D) Changes of released TNF-α and IL-6 protein from AML-12 cells and cellular TNF-α and IL-6 protein of AML-12 cells treated with ethanol/PA in the absence or presence of MLT, and KD of *Tert* (*n* = 4 for ELISA results; *n* = 3 for Western blotting). (E) Quantitative PCR results of *Osm* and *Osmr*, and Western blotting results of PCNA and Cyclin D1 of AML-12 cells treated with ethanol/PA in the absence or presence of MLT, and KD of *Tert* (*n* = 4 for qPCR results; *n* = 3 for Western blotting). Data are expressed as mean ± SD. *$P < 0.05$, **$P < 0.01$, ***$P < 0.001$ between indicated groups. For the quantification of Western blot, *$P < 0.05$, **$P < 0.01$, ***$P < 0.001$ *vs.* the scramble group; [#]$P < 0.05$, [##]$P < 0.01$, [###]$P < 0.001$ *vs.* the *Tert* siRNA group. Scale bar: 50 μm.

of endogenous *Tert* aggravated ethanol-induced serum damaging parameters, and impaired MLT-mediated improvement in ALD mice, including ALT, AST, TC, TG (Fig. 6B). Consistently, when compared with scramble shRNA transfected ALD mice, AAV8-sh*Tert* transfected ALD mice exhibited significantly severer hepatic histological injury, lipid accumulation, and higher liver triglyceride/pro-inflammatory cytokine levels (Fig. 6C−E). Knock-down of *Tert* did not alter the phosphorylation levels of both EGFR and Akt, but significantly impaired the regulation of

BRG1 and Cyclin D1 by MLT co-treatment in ALD mice, implying that downstream BRG1−TERT alteration had no influence in upstream EGFR−Akt signaling (Fig. 6F). Protein level changes of apoptosis, inflammation, and lipid metabolism markers also confirmed this finding (Fig. 6F). We also knocked-down hepatocyte-specific EGFR expression using the same strategy in ALD mice (Supporting Information Fig. S4A). Deficiency of *Egfr* slightly, yet not significantly, protected mice against ethanol-induced injury. Of note, MLT co-treatment mediated protection
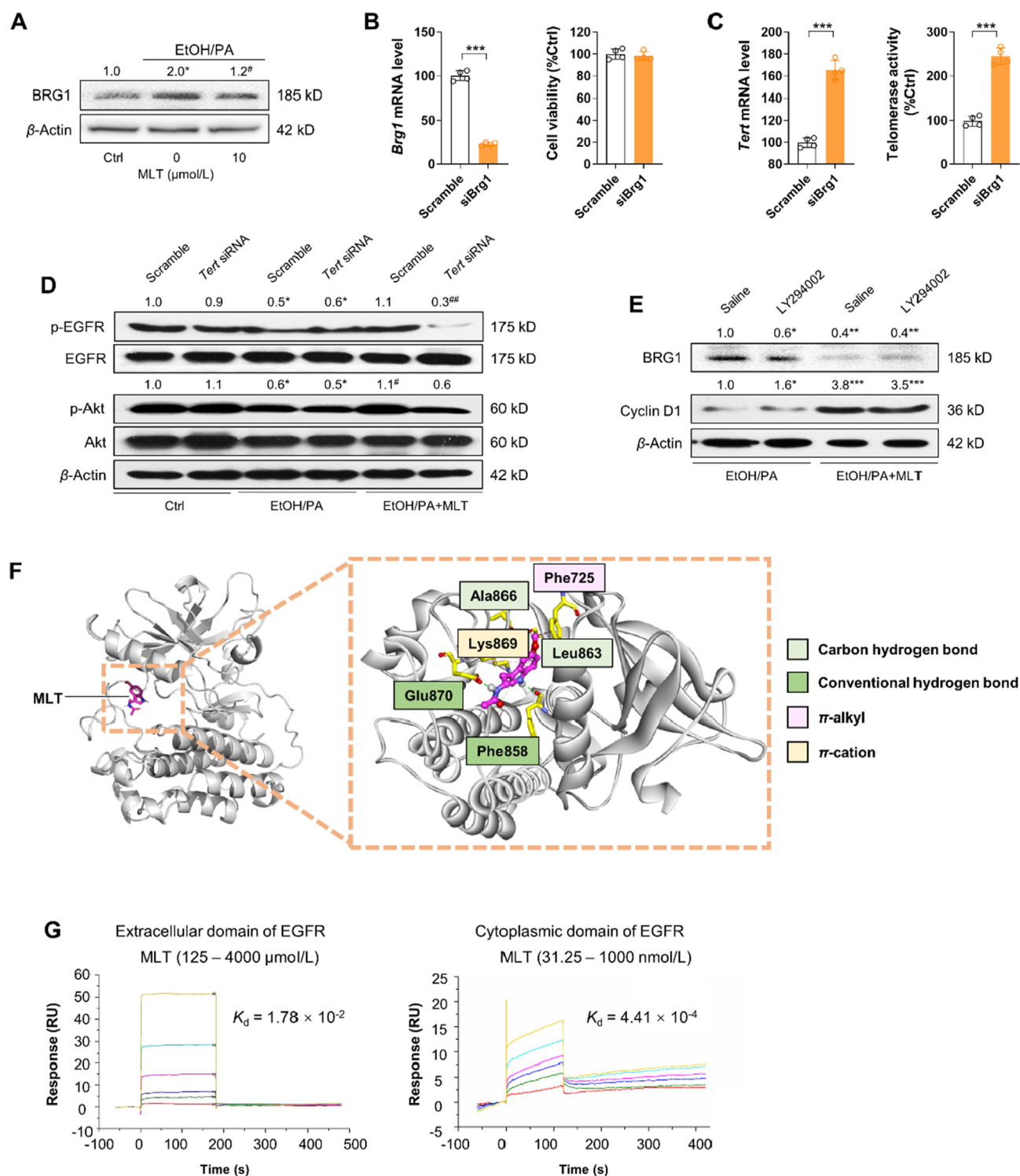
Figure 4 Epidermal growth factor receptor (EGFR) is the direct binding receptor of MLT to induce downstream Akt-BRG1 pathway. (A) Protein level change of BRG1 of AML-12 cells treated with ethanol/palmitate acid (PA) and MLT ($n = 3$). (B) Knock-down efficiency test of *Brg1* in AML-12 cells and subsequent cell viability influence (by siRNA, 24 h; $n = 4$). (C) Changes of *Tert* mRNA and cell telomerase activity after *Brg1* knock-down in AML-12 cells ($n = 4$). (D, E) Western blotting results of phosphorylated EGFR, total EGFR, phosphorylated Akt, total Akt, BRG1, and Cyclin D1 in AML-12 cells treated with ethanol/PA and ethanol/PA + MLT, with or without *Tert* knock-down ($n = 3$). (F) Molecular modeling analysis of MLT to the catalytic binding site of EGFR kinase domain. Left: Whole view of MLT to the binding site of EGFR (cartoon). Right: close-up view of MLT to the binding sites of EGFR (surface). (G) Surface plasmon resonance (SPR) assay exhibited the direct binding between different doses of MLT and eukaryotic recombinant murine EGFR protein (either the extracellular domain or the cytoplasmic domain) when co-incubated. Data are expressed as mean ± SD. ***$P < 0.001$ between indicated groups. For the quantification of Western blot, *$P < 0.05$, **$P < 0.01$ vs. the ctrl group; #$P < 0.05$, ##$P < 0.01$ vs. the EtOH group.
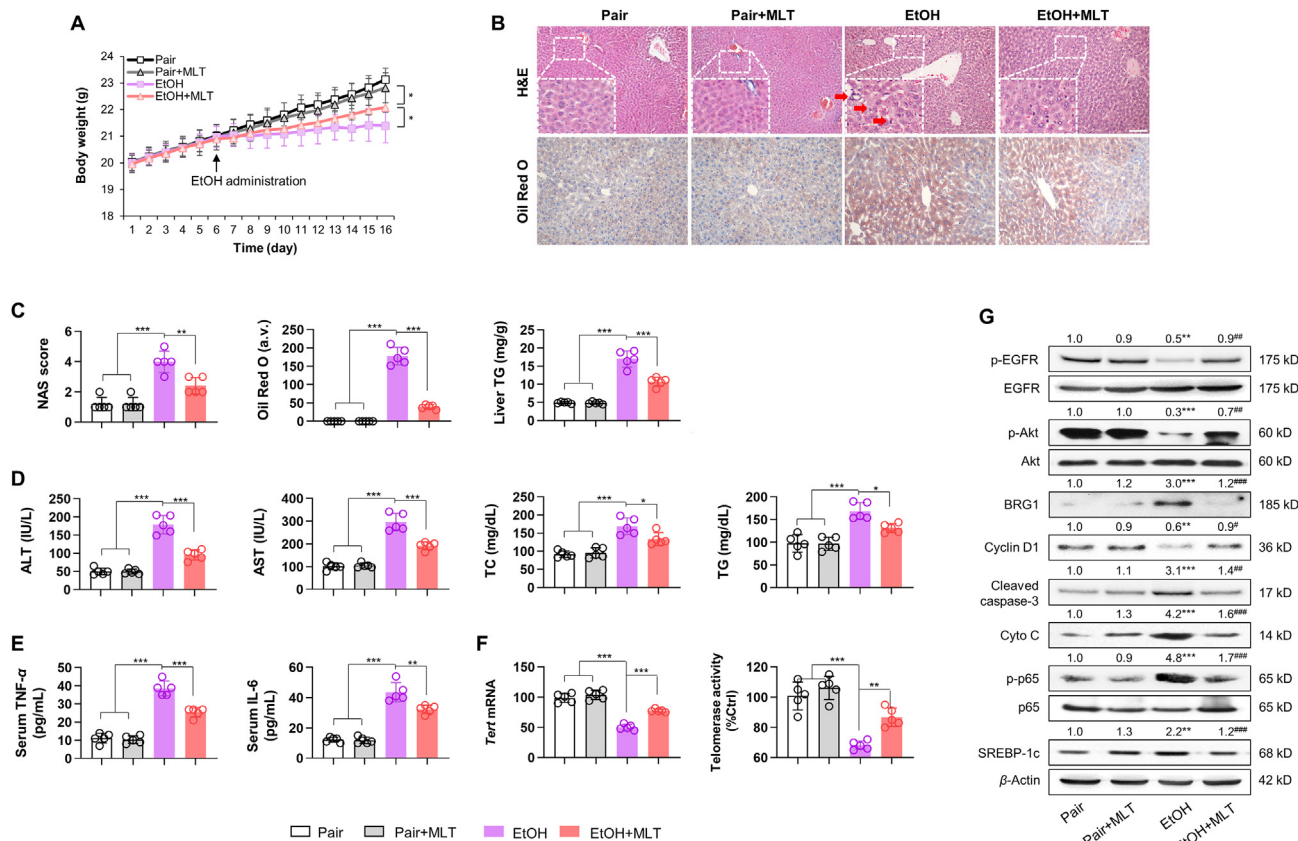
Figure 5 MLT improves liver injury in a mice chronic-binge alcoholic liver disease (the NIAAA) model. (A) MLT partially recovered reduced body weight of mice by ethanol administration from Day 6 to Day 16 ($n = 5$). (B) Representative liver H&E and Oil Red O staining results from mice with ALD and/or MLT co-treatment. (C) Changes of NAS (NAFLD activity score), Oil Red O quantification (arbitrary value; a.v.), and liver triglyceride (TG) from mice with ALD and/or MLT co-treatment ($n = 5$). (D) Changes of serum biochemical parameters [ALT, AST, total cholesterol (TC), and TG] from mice with ALD and/or MLT co-treatment ($n = 5$). (E) Changes of serum inflammatory mediators [tumor necrosis factor-alpha (TNF-α) and interleukin-6 (IL-6)] from mice with ALD and/or MLT co-treatment ($n = 5$). (F) Changes of *Tert* mRNA and hepatic telomerase activity from mice with ALD and/or MLT co-treatment ($n = 5$). (G) Protein level changes of phosphorylated EGFR, total EGFR, phosphorylated Akt, total Akt, BRG1, Cyclin D1, cleaved caspase-3, cytochrome *c* (Cyto C), phosphorylated NF-κB subunit p65, total p65, and SREBP-1c in the liver from mice with ALD and/or MLT co-treatment ($n = 3$). Data are expressed as mean $\pm$ SD. *$P < 0.05$, **$P < 0.01$, ***$P < 0.001$ between indicated groups. For the quantification of Western blot, *$P < 0.05$, **$P < 0.01$, ***$P < 0.001$ *vs*. the pair group; #$P < 0.05$, ##$P < 0.01$, ###$P < 0.001$ *vs*. the EtOH group. Scale bar: 50 μm.

was significantly impaired by *Egfr* knockdown in hepatocytes, including serum aminotransferases, liver lipid metabolism, and liver inflammatory cytokines (Supporting Information Fig. S4B−S4D). In terms of hepatic inflammation, we also checked the protein expression changes of TNF-α and IL-6 from WT, *Tert* conditional knockdown (CKD), and *Egfr* CKD mice liver lysates and got similar results with their serum expressional changes (Supporting Information Fig. S5). Collectively, our data showed that alleviation of MLT in ALD mice was partly through the EGFR−BRG1−TERT axis regulation.

3.6. Long-term MLT administration had no adverse effect on healthy mice

To facilitate future daily and/or clinical application of MLT in ALD prevention and treatment, we tested its possible toxicity in healthy mice after a 90-day administration. Male C57BL/6 mice (7-week-old) were daily gavaged with 10 mg/kg MLT for consecutively 90 days and we found no significantly change of the histology of the liver, kidneys, spleen, and hearts. In addition,

levels of serum ALT, AST, free fatty acid (FFA), and blood urea nitrogen (BUN) had no significant increase when compared with the control group (Supporting Information Fig. S6). These data indicated that long-term MLT administration had no adverse effect on healthy mice.

4. Discussion

Studies have demonstrated the health-promoting functions of MLT in a variety of liver disease models, including acute liver injury[41], NAFLD[42], liver fibrosis[43], and liver cancer[44]. Although studies suggested that MLT effectively alleviated ALD-induced liver injury *via* increased phosphorylation of AMPK, inhibited activation of NF-κB and possibly the MAPK−JNK/P38 signaling axis, the underlying mechanisms, particularly the direct binding receptor of MLT was largely unknown[45−47]. Based on our pilot study, we found that MLT effectively improved lipid accumulation, inflammation, apoptosis, and regeneration in cell and animal ALD models. RNA-seq analysis implied the crucial involving roles of TERT in ALD progression and MLT protection. In line
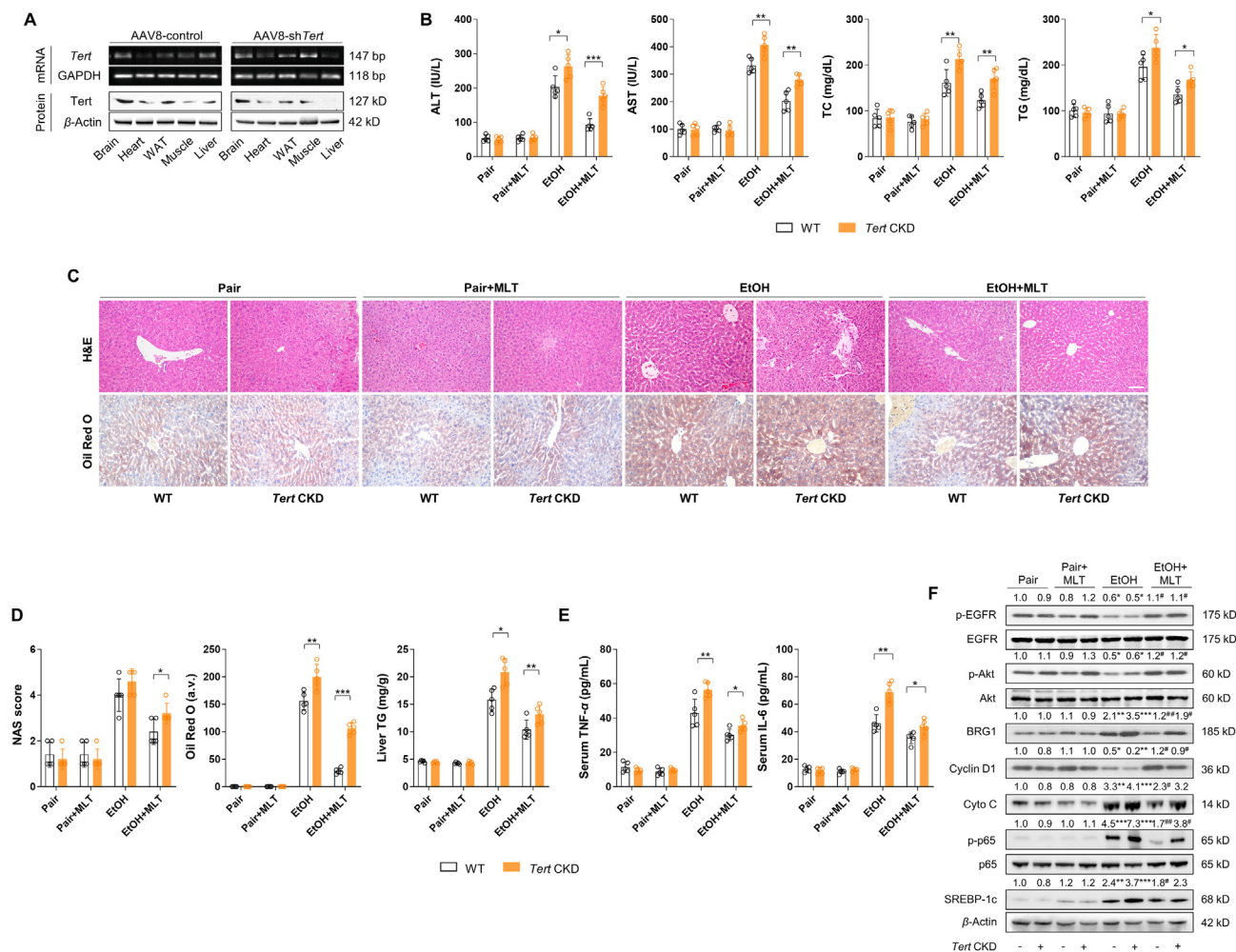
Figure 6 Liver-specific knock-down of *Tert* impairs MLT-mediated hepatoprotection in a mice chronic-binge alcoholic liver disease (the NIAAA) model. (A) AAV8-mediated *Tert* knock-down specificity in mice brain, heart, white adipose tissue (WAT), muscle, and liver, demonstrated by both PCR (mRNA level) and Western blotting (protein level). (B) Changes of serum biochemical parameters [ALT, AST, total cholesterol (TC), and TG] from wild-type and *Tert* conditional knock-down (CKD) mice with ALD and/or MLT co-treatment ($n = 5$). (C) Representative liver H&E and Oil Red O staining results from wild-type and *Tert* CKD mice with ALD and/or MLT co-treatment. (D) Changes of NAS (NAFLD activity score) and liver triglyceride (TG) from wild-type and *Tert* CKD mice with ALD and/or MLT co-treatment ($n = 5$). (E) Changes of serum inflammatory mediators [tumor necrosis factor-alpha (TNF-α) and interleukin-6 (IL-6)] from wild-type and *Tert* CKD mice with ALD and/or MLT co-treatment ($n = 5$). (F) Protein level changes of phosphorylated EGFR, total EGFR, phosphorylated Akt, total Akt, BRG1, Cyclin D1, cytochrome c (Cyto C), phosphorylated NF-κB subunit p65, total p65, and SREBP-1c in the liver from wild-type and *Tert* CKD mice with ALD and/or MLT co-treatment ($n = 3$). Data are expressed as mean $\pm$ SD. *$P < 0.05$, **$P < 0.01$, ***$P < 0.001$ between indicated groups. For the quantification of Western blot, *$P < 0.05$, **$P < 0.01$, ***$P < 0.001$ *vs.* the wild-type pair group; #$P < 0.05$, ##$P < 0.01$, ###$P < 0.001$ *vs.* the wild-type EtOH group. Scale bar: 50 μm.

with that, deficiency of *Tert* significantly impaired MLT-mediated hepatic improvements, both *in vitro* and *in vivo*. Previous research also suggested that exogenous MLT treatment increased telomerase activities in both young and aged rats, by inhibiting the replicative cellular senescence and lipid peroxidation[48]. Mechanistically, it was demonstrated that, in a somatic cell nuclear transfer-derived embryo model, MLT inhibited gene silencing-related heterochromatic epigenetic modification, such as DNA methylation and histone H3 lysine 9 trimethylation, to facilitate the enhancement of telomerase activity and telomere elongation[49]. Since BRG1 is a well-documented direct suppressor of *Tert* transcription for downstream signaling regulation, such as Wnt pathway and cell cycle pathways[36,50], we also demonstrated that BRG1 was up-regulated after ethanol treatment and suppressed by

MLT co-treatment, which were in opposite to the changing patterns of TERT. Moreover, knock-down of *Brg1* significantly increased both *Tert* expression and telomerase activity in hepatocytes, proving the interaction between BRG1 and TERT. This result was in line with recent reports that *Brg1* expression was up-regulated in the liver in mice fed with the methionine-choline deficient diet or after 70% partial hepatectomy[51,52].

It has been reported that ethanol-fed mice have higher levels of Kupffer cell TERT level than that of healthy mice[9], which seemed to be controversial to our data in hepatocytes after ethanol treatment. To clarify this phenotype discrepancy and to find out the upstream 'signal receiver' of BRG1/TERT, we selected EGFR as the target because (1) EGFR and BRG1 were found to be genetically antagonistic[37]; (2) EGFR had opposite functions in Kupffer

cells and in hepatocytes during liver cancer development and that the deletion of EGFR in macrophages inhibited hepatocellular carcinoma (HCC), whereas deletion of EGFR in hepatocytes promotes HCC[53]. EGFR is a critical regulator of hepatocyte proliferation and liver regeneration[54]. Its role in metabolic liver injury has been demonstrated in several reports. In a fast food diet model, pharmacological inhibition of EGFR by canertinib effectively prevents development of steatosis and liver injury, possibly *via* transcription factor (*e.g.*, peroxisome proliferator-activated receptor gamma and SREBP-1c) and Akt modulation[55]. In adult mice, mutation of EGFR significantly influences lipid metabolism in quiescent mouse liver also by SREBP regulation[56]. In cell models, ethanol suppresses EGFR autophosphorylation at Tyr1173 and Tyr1068, and downstream Akt activation[38]. In our ALD model, ethanol treatment also significantly inhibited the phosphorylation of both EGFR and Akt, which were partially recovered by the co-treatment with MLT. More important, by using biophysical and bioinformatics methods, we proved the binding between MLT and the cytoplasmic domain of EGFR, implying that EGFR was, at least one of the direct targets for MLT in the liver. In addition to *Tert* knock-down, we also suppressed endogenous *Egfr* expression in mice hepatocytes during ALD development. In agreement with the results from a NAFLD mice mode[55], although to a lesser extent, deficiency of *Egfr* slightly attenuated ALD phenotypes but almost abolished the hepatoprotective functions of MLT co-treatment. This result exhibited that EGFR was indeed a 'functional signal receiver and transducer' for MLT-mediated ALD protection. Admittedly, we did not test the involving roles of the endogenous MLT receptors (MT$_1$ and MT$_2$) in our ALD model because we did not observe significant changes of the AC−cAMP and PKC pathways when conducting the RNA-seq experiment and analysis. Since inhibition of the EGFR−BRG1−TERT axis could not fully abolish the effects of MLT on the mice liver, we cannot exclude the possible functions of the MT receptors.

5. Conclusions

Our study demonstrated that MLT was an effective and safe agent for liver injury alleviation in an ALD mice model. MLT directly bond and regulated hepatocyte surface EGFR to inhibit nuclear BRG1 activity, then enhance TERT expression, telomerase activity, and subsequent liver regeneration. Importantly, since abstinence often leads to severe and protracted sleep disruption (*e.g.*, insomnia) and MLT is found to improve sleep disturbance by shorting the time to fall asleep[57], it would be very meaningful to further investigate whether this hormone can be used as a diet supplement in alcoholics.

Authors contributions

Fei Wang and Jia Xiao conceived and designed the study; Zhaodi Che, Yali Song, Chengfang Xu, Wei Li, and Zhiyong Dong performed the experiments; Zhaodi Che, Wei Li, Zhiyong Dong, Cunchuan Wang, Yixing Ren, and Kwok-Fai So analyzed and interpreted the data. Zhaodi Che, George Lim Tipoe, Fei Wang, and Jia Xiao wrote the first draft of the manuscript and all authors revised the manuscript.

Conflicts of interest

The authors declare no conflicts of interest.

Appendix A. Supporting information

Supporting data to this article can be found online at https://doi.org/10.1016/j.apsb.2022.06.015.

References

1. Singal AK, Shah VH. Current trials and novel therapeutic targets for alcoholic hepatitis. *J Hepatol* 2019;**70**:305−13.
2. Xiao J, Wang F, Wong NK, He J, Zhang R, Sun R, et al. Global liver disease burdens and research trends: analysis from a Chinese perspective. *J Hepatol* 2019;**71**:212−21.
3. Xiao J, Wang F, Wong NK, Lv Y, Liu Y, Zhong J, et al. Epidemiological realities of alcoholic liver disease: global burden, research trends, and therapeutic promise. *Gene Expr* 2020;**20**:105−18.
4. Louvet A, Mathurin P. Alcoholic liver disease: mechanisms of injury and targeted treatment. *Nat Rev Gastroenterol Hepatol* 2015;**12**:231−42.
5. Lechel A, Manns MP, Rudolph KL. Telomeres and telomerase: new targets for the treatment of liver cirrhosis and hepatocellular carcinoma. *J Hepatol* 2004;**41**:491−7.
6. Nault JC, Ningarhari M, Rebouissou S, Zucman-Rossi J. The role of telomeres and telomerase in cirrhosis and liver cancer. *Nat Rev Gastroenterol Hepatol* 2019;**16**:544−58.
7. Alves-Paiva RM, Kajigaya S, Feng X, Chen J, Desierto M, Wong S, et al. Telomerase enzyme deficiency promotes metabolic dysfunction in murine hepatocytes upon dietary stress. *Liver Int* 2018;**38**:144−54.
8. Shi T, Yang X, Zhou H, Xi J, Sun J, Ke Y, et al. Activated carbon *N*-acetylcysteine microcapsule protects against nonalcoholic fatty liver disease in young rats *via* activating telomerase and inhibiting apoptosis. *PLoS One* 2018;**13**:e0189856.
9. Wu XQ, Yang Y, Li WX, Cheng YH, Li XF, Huang C, et al. Telomerase reverse transcriptase acts in a feedback loop with NF-κB pathway to regulate macrophage polarization in alcoholic liver disease. *Sci Rep* 2016;**6**:18685.
10. Kennaway DJ. A critical review of melatonin assays: past and present. *J Pineal Res* 2019;**67**:e12572.
11. McMullan CJ, Schernhammer ES, Rimm EB, Hu FB, Forman JP. Melatonin secretion and the incidence of type 2 diabetes. *JAMA* 2013;**309**:1388−96.
12. Li DJ, Tong J, Li YH, Meng HB, Ji QX, Zhang GY, et al. Melatonin safeguards against fatty liver by antagonizing TRAFs-mediated ASK1 deubiquitination and stabilization in a β-arrestin-1 dependent manner. *J Pineal Res* 2019;**67**:e12611.
13. Bahrami M, Cheraghpour M, Jafarirad S, Alavinejad P, Asadi F, Hekmatdoost A, et al. The effect of melatonin on treatment of patients with non-alcoholic fatty liver disease: a randomized double blind clinical trial. *Compl Ther Med* 2020;**52**:102452.
14. Hu S, Yin S, Jiang X, Huang D, Shen G. Melatonin protects against alcoholic liver injury by attenuating oxidative stress, inflammatory response, and apoptosis. *Eur J Pharmacol* 2009;**616**:287−92.
15. Eagon PK. Alcoholic liver injury: influence of gender and hormones. *World J Gastroenterol* 2010;**16**:1377−84.
16. Søberg S, Andersen ES, Dalsgaard NB, Jarlhelt I, Hansen NL, Hoffmann N, et al. FGF21, a liver hormone that inhibits alcohol intake in mice, increases in human circulation after acute alcohol ingestion and sustained binge drinking at Oktoberfest. *Mol Metabol* 2018;**11**:96−103.
17. Xu A, Wang Y, Keshaw H, Xu LY, Lam KS, Cooper GJ. The fat-derived hormone adiponectin alleviates alcoholic and nonalcoholic fatty liver diseases in mice. *J Clin Invest* 2003;**112**:91−100.

18. Lobo IA, Harris RA. GABA_A receptors and alcohol. *Pharmacol Biochem Behav* 2008;**90**:90−4.

19. Szabo G, Dolganiuc A, Dai Q, Pruett SB. TLR4, ethanol, and lipid rafts: a new mechanism of ethanol action with implications for other receptor-mediated effects. *J Immunol* 2007;**178**:1243−9.

20. Luo P, Wang F, Wong NK, Lv Y, Li X, Li M, et al. Divergent roles of kupffer cell TLR2/3 signaling in alcoholic liver disease and the protective role of EGCG. *Cell Mol Gastroenterol Hepatol* 2020;**9**:145−60.

21. Wang F, Tipoe GL, Yang C, Nanji AA, Hao X, So KF, et al. *Lycium barbarum* polysaccharide supplementation improves alcoholic liver injury in female mice by inhibiting stearoyl-CoA desaturase 1. *Mol Nutr Food Res* 2018;**62**:e1800144.

22. Xiao J, Liong EC, Ling MT, Ching YP, Fung ML, Tipoe GL. S-Allylmercaptocysteine reduces carbon tetrachloride-induced hepatic oxidative stress and necroinflammation *via* nuclear factor kappa B-dependent pathways in mice. *Eur J Nutr* 2012;**51**:323−33.

23. Xiao J, Xing F, Liu Y, Lv Y, Wang X, Ling MT, et al. Garlic-derived compound *S*-allylmercaptocysteine inhibits hepatocarcinogenesis through targeting LRP6/Wnt pathway. *Acta Pharm Sin B* 2018;**8**:575−86.

24. Bustin SA, Benes V, Garson JA, Hellemans J, Huggett J, Kubista M, et al. The MIQE guidelines: minimum information for publication of quantitative real-time PCR experiments. *Clin Chem* 2009;**55**:611−22.

25. Bertola A, Mathews S, Ki SH, Wang H, Gao B. Mouse model of chronic and binge ethanol feeding (the NIAAA model). *Nat Protoc* 2013;**8**:627−37.

26. Luo P, Zheng M, Zhang R, Zhang H, Liu Y, Li W, et al. *S*-Allyl-mercaptocysteine improves alcoholic liver disease partly through a direct modulation of insulin receptor signaling. *Acta Pharm Sin B* 2021;**11**:668−79.

27. Brunt EM, Kleiner DE, Wilson LA, Belt P, Neuschwander-Tetri BA. Nonalcoholic fatty liver disease (NAFLD) activity score and the histopathologic diagnosis in NAFLD: distinct clinicopathologic meanings. *Hepatology* 2011;**53**:810−20.

28. Solon-Biet SM, Mitchell SJ, Coogan SC, Cogger VC, Gokarn R, McMahon AC, et al. Dietary protein to carbohydrate ratio and caloric restriction: comparing metabolic outcomes in mice. *Cell Rep* 2015;**11**:1529−34.

29. Zhao Y, Abreu E, Kim J, Stadler G, Eskiocak U, Terns MP, et al. Processive and distributive extension of human telomeres by telomerase under homeostatic and nonequilibrium conditions. *Mol Cell* 2011;**42**:297−307.

30. Gajiwala KS, Feng J, Ferre R, Ryan K, Brodsky O, Weinrich S, et al. Insights into the aberrant activity of mutant EGFR kinase domain and drug recognition. *Structure* 2013;**21**:209−19.

31. Pan B, Fang S, Zhang J, Pan Y, Liu H, Wang Y, et al. Chinese herbal compounds against SARS-CoV-2: puerarin and quercetin impair the binding of viral S-protein to ACE2 receptor. *Comput Struct Biotechnol J* 2020;**18**:3518−27.

32. Ouyang S, Song X, Wang Y, Ru H, Shaw N, Jiang Y, et al. Structural analysis of the STING adaptor protein reveals a hydrophobic dimer interface and mode of cyclic di-GMP binding. *Immunity* 2012;**36**:1073−86.

33. Gao B, Ahmad MF, Nagy LE, Tsukamoto H. Inflammatory pathways in alcoholic steatohepatitis. *J Hepatol* 2019;**70**:249−59.

34. Sirma H, Kumar M, Meena JK, Witt B, Weise JM, Lechel A, et al. The promoter of human telomerase reverse transcriptase is activated during liver regeneration and hepatocyte proliferation. *Gastroenterology* 2011;**141**:326−37. 37.e1-3.

35. Lin S, Nascimento EM, Gajera CR, Chen L, Neuhöfer P, Garbuzov A, et al. Distributed hepatocytes expressing telomerase repopulate the liver in homeostasis and injury. *Nature* 2018;**556**:244−8.

36. Park JI, Venteicher AS, Hong JY, Choi J, Jun S, Shkreli M, et al. Telomerase modulates Wnt signalling by association with target gene chromatin. *Nature* 2009;**460**:66−72.

37. Fillmore CM, Xu C, Desai PT, Berry JM, Rowbotham SP, Lin YJ, et al. EZH2 inhibition sensitizes BRG1 and EGFR mutant lung tumours to TopoII inhibitors. *Nature* 2015;**520**:239−42.

38. Ma C, Bower KA, Lin H, Chen G, Huang C, Shi X, et al. The role of epidermal growth factor receptor in ethanol-mediated inhibition of activator protein-1 transactivation. *Biochem Pharmacol* 2005;**69**:1785−94.

39. Zhao Y, Liu J, Cai X, Pan Z, Liu J, Yin W, et al. Efficacy and safety of first line treatments for patients with advanced epidermal growth factor receptor mutated, non-small cell lung cancer: systematic review and network meta-analysis. *BMJ* 2019;**367**:l5460.

40. An Z, Aksoy O, Zheng T, Fan QW, Weiss WA. Epidermal growth factor receptor and EGFRvIII in glioblastoma: signaling pathways and targeted therapies. *Oncogene* 2018;**37**:1561−75.

41. Cao Z, Fang Y, Lu Y, Tan D, Du C, Li Y, et al. Melatonin alleviates cadmium-induced liver injury by inhibiting the TXNIP−NLRP3 inflammasome. *J Pineal Res* 2017;**62**:e12389.

42. Zhou H, Du W, Li Y, Shi C, Hu N, Ma S, et al. Effects of melatonin on fatty liver disease: the role of NR4A1/D-NA−PKcs/p53 pathway, mitochondrial fission, and mitophagy. *J Pineal Res* 2018;**64**:e12450.

43. Kang JW, Hong JM, Lee SM. Melatonin enhances mitophagy and mitochondrial biogenesis in rats with carbon tetrachloride-induced liver fibrosis. *J Pineal Res* 2016;**60**:383−93.

44. Fernández-Palanca P, Méndez-Blanco C, Fondevila F, Tuñón MJ, Reiter RJ, Mauriz JL, et al. Melatonin as an antitumor agent against liver cancer: an updated systematic review. *Antioxidants* 2021;**10**:103.

45. Rui BB, Chen H, Jang L, Li Z, Yang JM, Xu WP, et al. Melatonin upregulates the activity of AMPK and attenuates lipid accumulation in alcohol-induced rats. *Alcohol Alcohol* 2016;**51**:11−9.

46. Sun H, Wang X, Chen J, Song K, Gusdon AM, Li L, et al. Melatonin improves non-alcoholic fatty liver disease *via* MAPK−JNK/P38 signaling in high-fat-diet-induced obese mice. *Lipids Health Dis* 2016;**15**:202.

47. Sato K, Meng F, Francis H, Wu N, Chen L, Kennedy L, et al. Melatonin and circadian rhythms in liver diseases: functional roles and potential therapies. *J Pineal Res* 2020;**68**:e12639.

48. Akbulut KG, Gonul B, Akbulut H. The role of melatonin on gastric mucosal cell proliferation and telomerase activity in ageing. *J Pineal Res* 2009;**47**:308−12.

49. Yang L, Liu X, Song L, Su G, Di A, Bai C, et al. Inhibiting repressive epigenetic modification promotes telomere rejuvenation in somatic cell reprogramming. *FASEB J* 2019;**33**:13982−97.

50. Wu S, Ge Y, Huang L, Liu H, Xue Y, Zhao Y. BRG1, the ATPase subunit of SWI/SNF chromatin remodeling complex, interacts with HDAC2 to modulate telomerase expression in human cancer cells. *Cell Cycle* 2014;**13**:2869−78.

51. Kong M, Chen X, Xu H, Wenping, Fang M, Xu Y. Hepatocyte-specific deletion of *Brg1* alleviates methionine-and-choline-deficient diet (MCD) induced non-alcoholic steatohepatitis in mice. *Biochem Biophys Res Commun* 2018;**503**:344−51.

52. Wang B, Kaufmann B, Engleitner T, Lu M, Mogler C, Olsavszky V, et al. Brg1 promotes liver regeneration after partial hepatectomy *via* regulation of cell cycle. *Sci Rep* 2019;**9**:2320.

53. Lanaya H, Natarajan A, Komposch K, Li L, Amberg N, Chen L, et al. EGFR has a tumour-promoting role in liver macrophages during hepatocellular carcinoma formation. *Nat Cell Biol* 2014;**16**:972−7.

54. Natarajan A, Wagner B, Sibilia M. The EGF receptor is required for efficient liver regeneration. *Proc Natl Acad Sci U S A* 2007;**104**:17081−6.

55. Bhushan B, Banerjee S, Paranjpe S, Koral K, Mars WM, Stoops JW, et al. Pharmacologic inhibition of epidermal growth factor receptor suppresses nonalcoholic fatty liver disease in a murine fast-food diet model. *Hepatology* 2019;**70**:1546−63.

56. Scheving LA, Zhang X, Garcia OA, Wang RF, Stevenson MC, Threadgill DW, et al. Epidermal growth factor receptor plays a role in the regulation of liver and plasma lipid levels in adult male mice. *Am J Physiol Gastrointest Liver Physiol* 2014;**306**:G370−81.

57. Thakkar MM, Sharma R, Sahota P. Alcohol disrupts sleep homeostasis. *Alcohol* 2015;**49**:299−310.